# Low-cycle fatigue lifetime prediction using a dislocation-based stage II crack plasticity model: Application to austenitic steels

Zhenyu Yang, Christian Robertson, Xianfeng Ma, Déprés Christophe

▶ **To cite this version:**

Zhenyu Yang, Christian Robertson, Xianfeng Ma, Déprés Christophe. Low-cycle fatigue lifetime prediction using a dislocation-based stage II crack plasticity model: Application to austenitic steels. Computational Materials Science, 2024, 243, pp.113144. 10.1016/j.commatsci.2024.113144 . cea-04604174

**HAL Id: cea-04604174**

**https://cea.hal.science/cea-04604174**

Submitted on 14 Jun 2024

**HAL** is a multi-disciplinary open access archive for the deposit and dissemination of scientific research documents, whether they are published or not. The documents may come from teaching and research institutions in France or abroad, or from public or private research centers.

L'archive ouverte pluridisciplinaire **HAL**, est destinée au dépôt et à la diffusion de documents scientifiques de niveau recherche, publiés ou non, émanant des établissements d'enseignement et de recherche français ou étrangers, des laboratoires publics ou privés.

# Low-cycle fatigue lifetime prediction using a dislocation-based stage II crack plasticity model: application to austenitic steels

Zhenyu YANG[a,*], Christian ROBERTSON[a], Xianfeng MA[b] and Christophe DÉPRÉS[c]

[a]Université Paris-Saclay, CEA, Service de Recherche en Matériaux et procédés Avancés, 91191, Gif-sur-Yvette, France
[b]Sun Yat-Sen University, 519082, Zhuhai, China
[c]Laboratoire SYstemes et Matériaux pour la MEcatronique, Université de Savoie, BP80439, 74944, Annecy-le-Vieux Cedex, France

ARTICLE INFO

*Keywords*:
fatigue
stage II cracks
dislocations
stochastic life prediction
316L stainless steel

ABSTRACT

Low-cycle fatigue damage is examined using a specific theoretical Stage II crack growth model, adapted to series 300 austenitic steels. This method builds upon previous 3D Dislocation Dynamics (DD) studies, deriving an expression for crack growth rate ($da/dN$) that incorporates the cyclic plasticity mechanisms governing grain-scale Crack-Tip Opening Displacement (CTOD). The objective of this research is to assess the efficacy of this particular model in predicting Stage II crack growth across macroscopic poly-crystals. The transition from microscale (grain) to macroscale is facilitated through a distinct procedure, which involves systematic variation of the sub-grain model inputs using relevant polycrystalline EBSD data. The outcomes of these calculations are presented as fatigue crack growth rate plots and fatigue lifetime plots. The findings align with pertinent experimental observations within the LCF regime, both in terms of absolute values and variability. The methodology employed here seeks to provide robust quantitative data to bolster fatigue design activities, particularly within the context of fusion reactor technology.

## 1. Introduction

Structural nuclear materials including series-300 steels are exposed to fatigue loading conditions. In such materials, fatigue damage usually evolves according to the following course of events. Cyclic first gives rise to strain localization in the form of persistent slip bands (PSBs) [1–3]. Active PSBs generate irreversible surface displacements called persistent slip markings (PSMs). PSMs may take the form of extrusions that keep growing during Stage 0, up to the nucleation of a (sub-micron) crack-like discontinuity. Such initial defects then develop and cut through the primary grains during Stage I, up to the first microstructural barrier (grain boundary). Stage I crack propagation mainly occurs at the PSB-matrix interface [3–5] or within the PSB itself [5, 6], i.e., parallel to a specific crystallographic slip plane [7]. Stage I cracks getting past the first barrier become Stage II cracks, which then grow up to the complete specimen failure.

Stage II fatigue cracks and related cyclic plasticity mechanisms were investigated under various realistic grain-scale configurations, using dislocation dynamics (DD) simulations [8]. These investigations return $da/dN$ expression similar to the Paris' law; albeit working with a set of physical variables instead of the usual empirical coefficients (see section 2.1). Our goal in this work is to evaluate the ability of that particular model to predict Stage II-related low-cycle fatigue lifetime at the scale of macroscopic poly-crystals. The scale transition from crack-tip plasticity to macro-scale poly-crystals is here addressed using a specific calculation procedure; where the input model variables are systematically varied according to applicable EBSD data (grain size and orientation). The present modeling effort is more generally aimed at assisting the fatigue design whenever the supporting data is inaccessible or unavailable.

This paper is organized as follows. Section 2.1 recalls the principles of our specific Stage II crack propagation model and the physical interpretation of its constitutive parameters. Section 2.2 presents the calculation method treating the crack-tip to poly-crystalline scale transition in terms of fatigue damage. The corresponding model evaluation results are presented in section 3, in the form of theoretical $a-N$, $da/dN-\Delta K$ and fatigue lifetime versus load plots. The effect of a broad range of loading conditions on Stage II propagation is evaluated by comparison with applicable experimental evidence, each time possible.

*Corresponding author
*Email address:* yang-zhenyu@outlook.com (Z. YANG)
ORCID(s): 0000-0001-5480-7123 (Z. YANG)

## 2. Simulation methods

### 2.1. Fatigue lifetime model based on dislocation-mediated cyclic plasticity mechanisms

This paper features an original stage-II crack propagation model, accounting for dislocation-mediated plasticity mechanisms revealed by prior, three-dimensional (3D) dislocation dynamics (DD) simulations [8–11]. Those specific investigations provide invaluable insight into the local, grain-scale dislocation displacement and multiplication mechanisms pertaining to grade 300 austenitic steels. One typical, three-dimensional DD simulation setup utilized is shown in Fig. 1 below, which explicitly combines:

i a set of (two) free surfaces inserted in a grain, embedded in an elastic matrix representing the surrounding, un-cracked grain matrix or medium,
ii a heterogeneous, crack-induced stress field (not shown) [6],
iii a set of random dislocation sources placed at a short distance ahead of the crack tip surfaces [7]. These sources produce plastic strain everywhere in the grain (owing to dislocation multiplication and subsequent glide), including in the crack tip region.

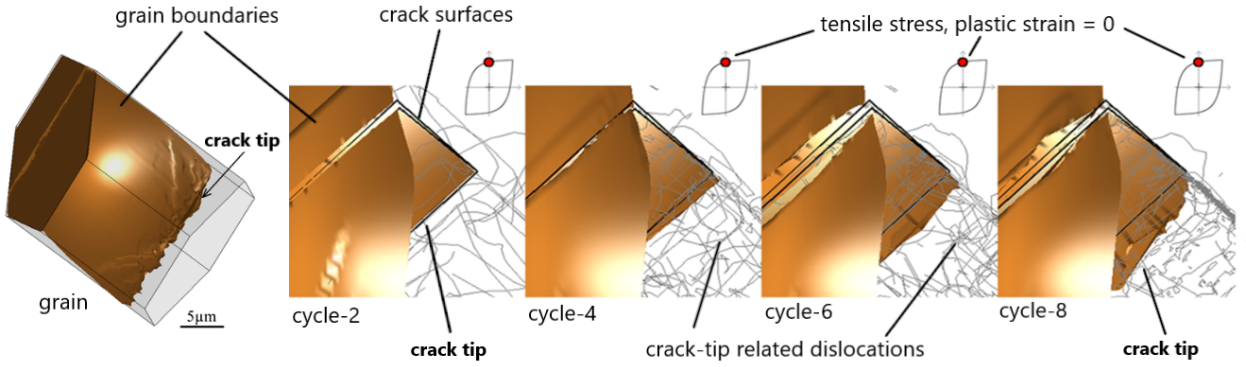


**Figure 1:** Dislocation-mediated cyclic plasticity mechanisms associated with Stage II cracks. The simulation setup presented is representative of a 3D Stage II crack microstructure. The simulation shown is carried out in under imposed plastic strain range $2 \times 10^{-4}$ using symmetrical ($R = -1$) loading conditions. The snapshots shown are taken at different cycle numbers, at exactly the same reference plastic strain conditions, for accurate evaluation of the surface displacement time evolutions. Such surface displacement maps are used to develop the CTOD expressions Eq. (1) - Eq. (3) used in this paper.

The above-described DD investigations are carried out with a view to accurately map out the crack-tip displacements field and its evolutions with the number of fatigue cycles, using the calculation method prescribed in [12]. It is thereby found that tip-related cyclic plasticity is mostly homogeneous and usually involves multiple slip systems, up until the crack-tip approaches the grain boundary barriers ($a_g / D_g \geq 0.8 - 0.9$ where $a_g$ is the crack length in the grain containing the crack tip). The crack-emitted dislocations then strongly interact with the grain boundaries, which transiently affects the crack growth rate [7, 11].

Additional DD investigations were undertaken with a view to developing an innovative, physically-based Stage II crack growth model. These investigations treated two important scale transition effects. The first one considers the grain scale stress-strain state conversion into micro-scale, crack-tip displacements, which can be accurately described using Eq.7 from reference [8]. The second scale transition regards the crack-tip-related strain transfer to macroscopic plastic strain noted as $\Delta\epsilon_{p,local} \rightarrow \Delta\epsilon_{p,macro}$. This effect can be described using Eq. 9 in reference [8], where $\Delta\epsilon_{p,local}$ asymptotically tends to a finite, minimal value as $\Delta\epsilon_{p,macro}$ vanishes. The latter expression is established by comparing the cyclic stress-strain response of cracked versus uncracked grains, using different (with and without crack) DD simulation cases [13]. Combining Eqs. (7) and (9) from reference [8] allows obtaining a general CTOD description applicable to Stage II crack propagation, including macroscopic loading variables and relevant microscopic physical parameters. That expression writes (see also Table 1 and the following text below):

$$\frac{da}{dN} = C\Delta K_{app}^2 F^2 \tag{1}$$

**Table 1**
Material constants for fatigue life prediction in grade 300 austenitic steel.

| Parameter | Value | Physical meaning |
|---|---|---|
| S | 0.66 | The grain shape factor applicable to equiaxial grains [14] |
| $\mu$ | $8.4 \times 10^{10}\ Pa$ | Shear modulus |
| $\nu$ | 0.3 | Poisson's ratio |
| $\lambda$ | 25 | the (dimensionless) number of active (mobile) dislocations in an $r_0$ large crack-tip process zone [15] |
| $b$ | $2.5 \times 10^{-10}\ m$ | Burgers vector |
| $\sigma_{crit}(D_g, \Delta\sigma_{app}, \gamma_{surf})$ | $14.4\ MPa$ | Critical nano-cavity nucleation stress at the crack tip, used to calculate $N_i$ and detailed in [8], section 4.2 |
| $\gamma_{surf}$ | $1.3{\times}10^{-3}\ J/m^2$ | Surface energy, environment and temperature dependent |
| $\Delta K_0$ | $1\ MPa\sqrt{m}$ | Reference unit stress intensity factor, its value is fixed to $1\ MPa\sqrt{m}$ |

where $\Delta K_{app} = \sigma_{app}\sqrt{\pi a}$ whereas:

$$C = \frac{D_g}{2r_0(\frac{1}{S}\frac{\mu}{1-\nu})\Delta\sigma_{app}N_i} \tag{2}$$

and

$$F = \sqrt{1 - exp(\frac{r_0(\frac{1}{S}\frac{\mu}{1-\nu})\Delta\sigma_{app}}{K_0^2}\frac{\lambda b}{2D_g})} \tag{3}$$

The physical interpretation of the variables appearing in Eq. (2) and Eq. (3) is as follows:

- $C$ (in $MPa^{-2}$ units) characterizes the material resistance against the crack front extension.
- $F$ is a dimensionless efficiency factor, tuning the local (grain-scale) crack growth rate since $\Delta K_{app}^2 F^2 = \Delta\sigma_{app}^2 \pi a F^2$ is proportional to the elastic energy driving the crack growth.
- $\Delta\epsilon_{p,macro}$ is the applied plastic strain range (tension plus compression)
- $\Delta\sigma_{app}$ is the applied stress range, calculated from the Ramberg-Osgood relation according to $\Delta\epsilon_{p,macro}$.
- $D_g$ is the effective grain size in reference to Fig. 2.
- $N_i$ is the time to initiation of a micro-cavity (in cycles) at the tip of the crack from solving Eq. (4). Quantity $N_i$ directly tunes up the number of cycles for the crack to grow by one CTOD-wide strip deeper and therefore, the material's resistance to crack extension. Additional qualitative explanations are given in the following paragraphs whereas a thorough quantitative application is presented in [8].

The above-listed variables generally depend on either the loading conditions or the evolution of the grain-scale microstructure. The (invariable) material constants used in the model are listed in Table 1.

It is important to note that the dislocation-mediated slip irreversibility (from 1% to about 5% based on DD simulations from [14]) appears much too small to explain the crack growth rate observed in 300-series steels [8]. This outcome points to an alternate crack advance scenario including the sudden, periodic emission of nano-cavities in the crack-front region [11] following a similar idea presented in [16] and further explored in Section 3.8 of [17].

It is important to note that, the above crack growth scenario is entirely compatible with the formation of fatigue striations in the fracture surface [18], since $N_i >> 0.25$ (i.e. much longer than one tensile or compressive stroke, as discussed hereafter) and nano-cavity size $a <<$ striation-width (i.e. typically several microns). In these conditions, multiple surface step-in and step-out sequences occur in the crack tip region before any permanent crack advance actually takes place. Step-out events are concurrent with the absorption of various molecules ($H_2O$, $N_2$, $O_2$, $H_2$,

etc) present in the testing environment (e.g. in air, at room temperature). The subsequent step-in occurrence (upon load reversal) then assists the adsorbed molecule transport inside the crystal, thereby causing the embrittlement of the step-in/step-out region. Reversible step-in/step-out sequences thus proceed until a permanent nano-cavity is initiated, somewhere along the crack front. The newly nucleated nano-cavity then promotes the rapid de-cohesion of the much larger, adjacent brittle region, whereas a sharp striation contrast is produced in the fracture surface, in concurrence with the emission of a strong acoustic signal [19, 20]. That scenario explains how a sharp, discontinuous striation contrast is produced together with continuous, reversible dislocation glide characterizing low-SFE metals (including series 300 steels). This nano-cavity formation mechanism is noteworthy not equivalent to striation formation itself but rather, with striation initiation. The present sequence of events is also coherent with a marked difference in crack propagation rate for experiments of fatigue in air and vacuum [21–23].

Nano-cavity nucleation is, in principle, a highly non-equilibrium phenomenon with complex spatiotemporal character [24]. The present, simplified approach is based on detailed, sub-grain scale stress-energy evolution analysis showing that stress-energy conditions compatible with cavity nucleation are periodically satisfied, within the dislocation sub-structures of a persistent slip band [17]. In our model, the rate of micro-cavity nucleation directly affects the Stage II crack growth rate through quantity $N_i$. In practice, quantity $N_i$ is evaluated during each cycle using the following stress-energy balance equation:

$$\sigma_0 + (\frac{\partial \sigma_{int}(D_g,\, \Delta\sigma_{app})}{\partial N})N_i = \sigma_{crit}(D_g,\, \Delta\sigma_{app},\, \gamma_{surf}) \tag{4}$$

- Quantity $\sigma_{crit}(D_g,\, \Delta\sigma_{app},\, \gamma_{surf})$ is evaluated using Griffiths' expression and interpreted as the effective, critical nano-cavity nucleation stress depending on critical surface energy $\gamma_{surf}$ [25–28];
- $\sigma_0 \approx 0$ (once formed, the nano-cavity is permanent)
- $\partial\sigma_{int}(D_g,\, \Delta\sigma_{app})/\partial N$ the internal stress rate of evolution due to crack tip plasticity mechanisms (see Table 1).
- Quantity $\partial\sigma_{int}(D_g, \Delta\sigma_{app})/\partial N$ depends on equivalent dipole height evolution $dy/dN$. Both quantities can be evaluated using DD simulations, returning $\partial\sigma_{ini}(D_g, \Delta\sigma_{app})/\partial N = 5 - 12\ MPa/cycle$ and $dy/dN = 1.5 - 6\ nm/cycle$ [11].

The above parameters all depend on the grain size $D_g$ and the loading condition, they will be evaluated at each cycle and produce a different $N_i$ for each fatigue cycle.

### 2.2. Experimental data for stochastic fatigue lifetime evaluation

This Section presents the supporting data allowing Stage II crack growth description/prediction at the macroscopic scale. In practice, the Stage II crack growth rate is evaluated by varying Eqs. (1) to (4) entries according to grain size and grain orientation data collected in an actual grain aggregate c.f. Fig. 2. The *effective grain size* assigned to each EBSD data point is: $D_g^{eff} = M_\theta \delta$ where $M_\theta$ is the number of consecutive measurements yielding $\theta \leq 5°$ along a given raster scan line (horizontal X-axis in Fig. 2a) and $\delta = 0.5\ \mu m$ is the measurement step. It is assumed that $D_g^{eff}$ is a fair approximation of the (maximal) gliding distance of dislocation lines sitting in a given grain, at or near the calculation point considered. In the rest of the paper, reference to *grain size* will regard to $D_g^{eff}$ unless otherwise specified.

## 3. Results

This Section presents Stage II crack propagation calculations applicable to typical series 300 steel, polycrystalline aggregates. An effective grain size is initially attributed to each EBSD measurement point or data pixel. It is then assumed that stage II cracks cut through the grain aggregate along the EBSD scan lines, i.e., perpendicular to the loading axis (along AB or CD segments, for example: see Fig. 2a), in agreement with corresponding observations (c.f. uni-axial fatigue tests). We then calculate the number of cycles corresponding to each crack length increment using Eqs. (1) to (4) using the materials parameters listed in Table 1 below, for typical experimental fatigue cases.

Acceleration and deceleration of the individual crack growth rate is visible in Figs. 3a and 3b and is directly ascribed to the local grain size and orientation variations, as Stage II cracks grow and cut through the polycrystalline aggregate. Namely, Stage II cracks grow faster where the effective grain size is larger and conversely slower where the active or

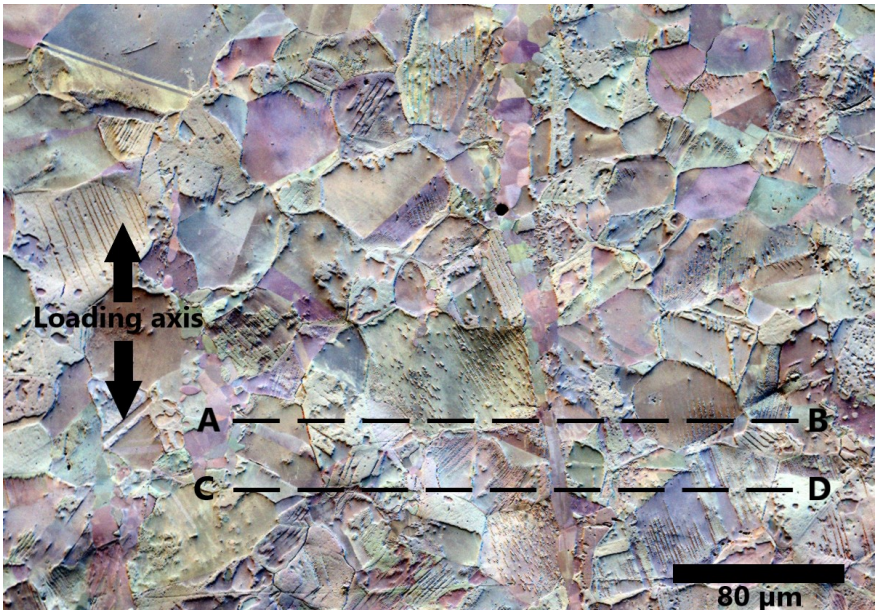


(a)

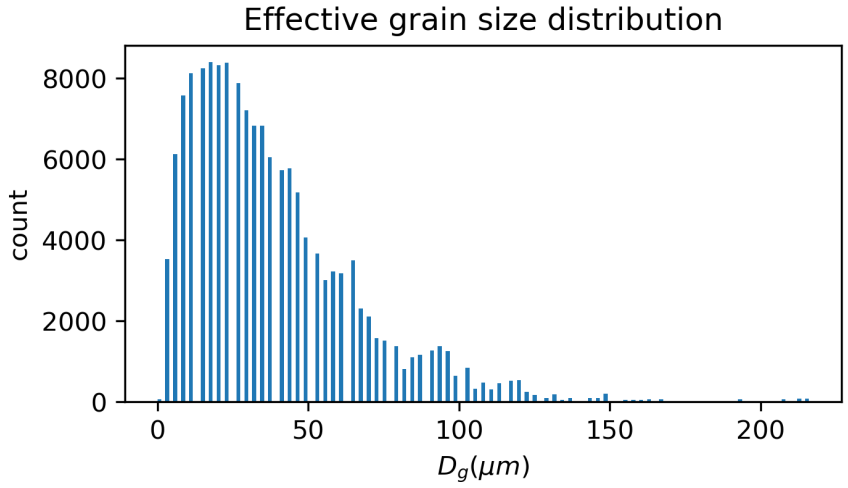


(b)

**Figure 2:** Model grain aggregate used for stochastic fatigue lifetime prediction. (a) Typical surface grains aggregate of a grade 300 austenitic steel specimen. Markers A-B and C-D show two possible crack propagation paths, consistent with the loading axis indicated. (b) Effective grain size distribution of the above-displayed grain aggregate.

resisting grain size is smaller (compare Figs. 3a and 3b). This means that poly-crystalline grain size and orientation dispersion itself possibly have a major effect in terms of Stage II crack-growth scattering.

We then attempt to evaluate the crack growth rate scattering effect accounting for a macroscale grain aggregate in a broad range of loading conditions ($\Delta\epsilon_p$ varies from $10^{-4}$ to $10^{-2}$) in symmetrical tension-compression $R = -1$. The corresponding stress range is calculated using the cyclic stress-strain curve applicable to 316L stainless steel, including both the tensile and compressive parts of the fatigue cycles. In practice, Stage II crack propagation through a grain aggregate c.f. Fig. 2a is evaluated using the calculation procedure detailed in Fig. 4 below.

The adopted calculation procedure also implicitly assumes that:

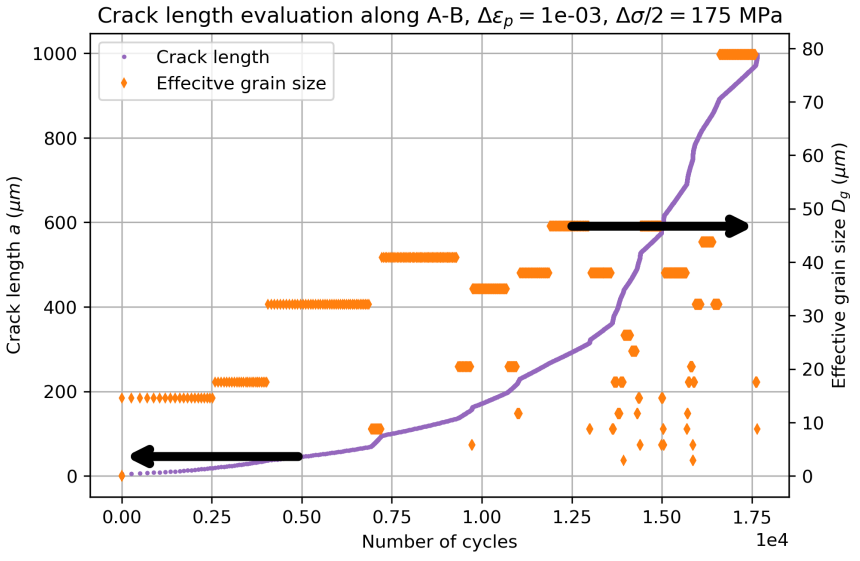


(a)

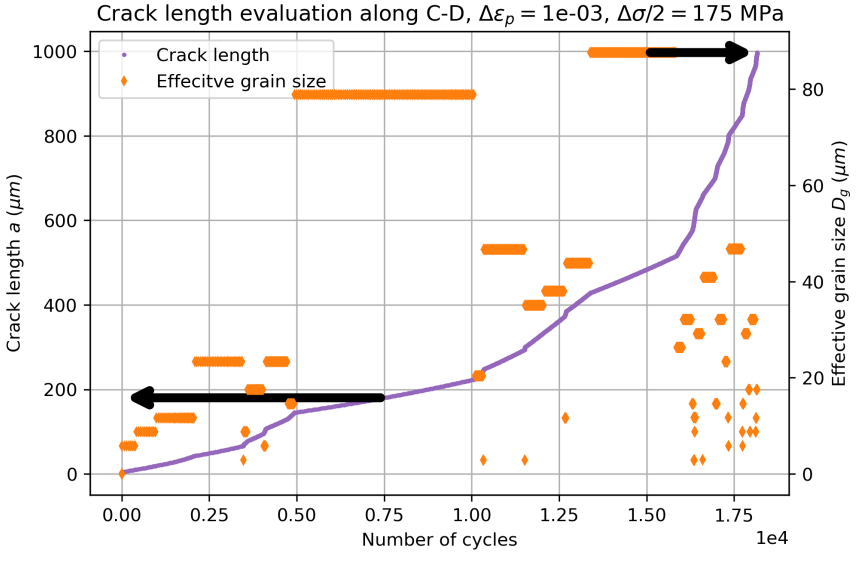


(b)

**Figure 3:** The solid orange symbols indicate the size of the grain being cut by the crack tip, at a given number of cycles. The solid purple curve indicates the corresponding crack length, at the same number of cycles. It is interesting to note the correlation between the grain size changes and the significant corresponding crack growth rate variations. (a) Crack length evolution along individual crack path A-B shown in Fig. 2a. (b) Crack length evolution along individual crack path C-D shown in Fig. 2a.

1. plastic strain range $\Delta\epsilon_{p_{macro}}$ and related applied stress range $\Delta\sigma_{app}$ remain constant as the cracks grow along their pre-assigned paths, throughout in the grain aggregate.
2. each calculated crack path is independent, i.e., the actual crack-to-crack distance is large enough to prevent mutual elastic interaction everywhere in the grain aggregate.
3. the mutual grain-to-grain interactions effect on $\Delta\sigma_{app}$ are negligible, which implies that grains of identical size, geometry, and orientation undergo the same tip-related plasticity mechanisms regardless of the neighboring grain environment. The grain environment effect can be regarded as short-ranged applied stress perturbation in the

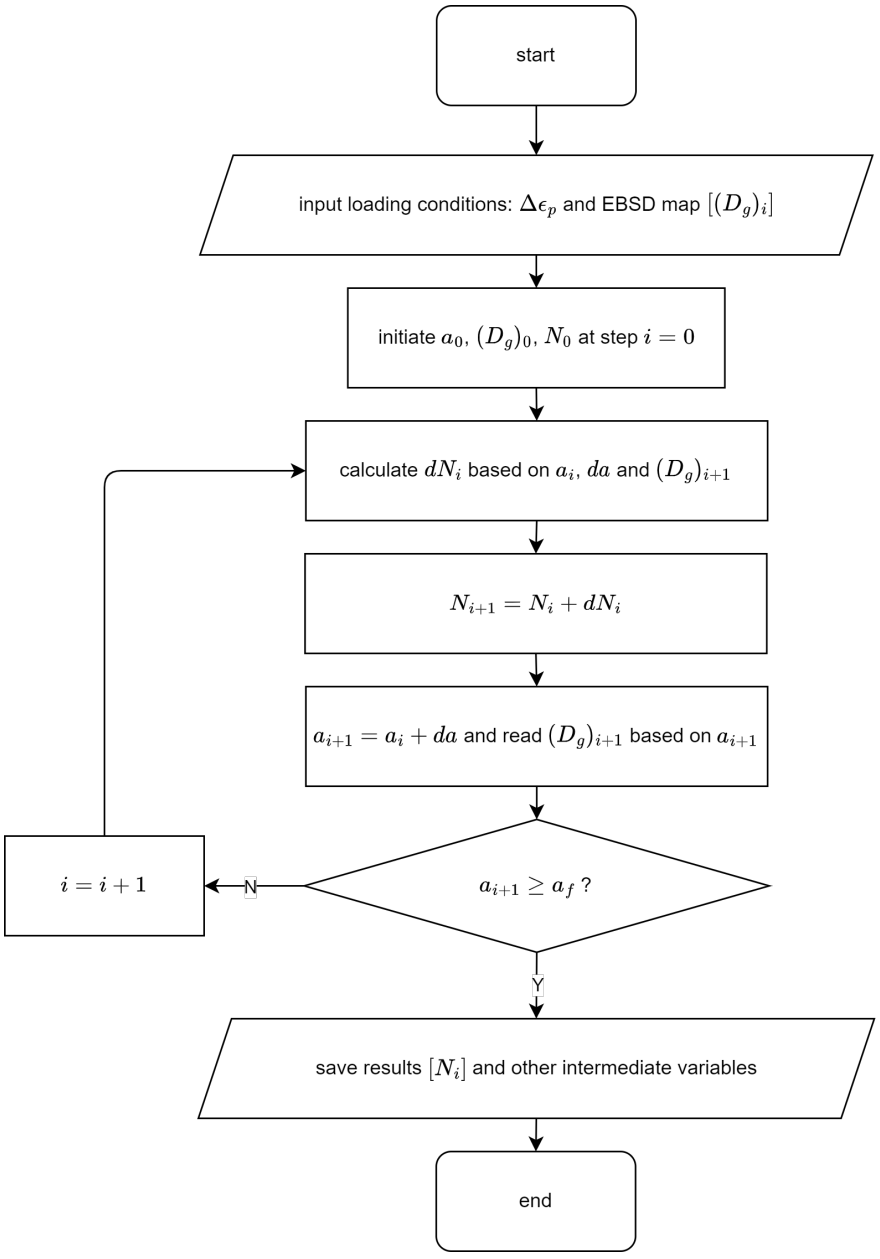


**Figure 4:** Detailed calculation procedure allowing the micro to macro scale transition. The flow chart shows the calculation procedure for a single crack path which is repeated for each pre-assigned crack path in the grain aggregate. Note that the calculation step is not based on the number of cycles increment $dN$ but on the crack length increment $da$.

crack-tip region. Perturbation amplitude no larger than 40% of the primary stress and has practically no effect on the cyclic plasticity evolution at the sub-grain scale [17]. The results thus support neglecting the mutual grain incompatibility effect in the particular context of crack tip plasticity.

Standard crack growth versus load plots or $\frac{da}{dN} - \Delta K$ are then generated and compared side by side with corresponding observation results (see Fig. 5). The main fatigue data validation set shown in Fig. 5 and Fig. 6 is obtained using the "FABIME" testing device [29], which utilizes quasi-structural disk specimens (diameter = 170 *mm*, 2 *mm* thickness in central gauge region) subjected to alternating bending displacements (e.g. total imposed strain conditions). The present FABIME tests are carried out at room temperature using an optically transparent and chemically inert oil as a working

fluid. Symmetrical disk bending displacement amplitudes up to 2.75 *mm* are applied, with corresponding strain ratio $R = -1$ and $\Delta\epsilon_p = 9.6 \times 10^{-3}$. The tests were interrupted every 500 cycles for the evaluation of the surface crack length $a$ (resolution limit is 50 $\mu m$). The test ran up to 19680 applied cycles yielding multiple crack development, in the specimen gauge section [30].

The equivalent stress range $\Delta\sigma_{app}$ acting in the specimen surface is evaluated using elastoplastic FEM fatigue calculations in consistence with the test condition executed [31]. It can be shown that the measured crack growth rate (see Fig. 5) is consistent with the Paris' rule description, using the room temperature empirical coefficients of series-300 steel and $\Delta K = \sqrt{\sigma_{app}\pi a}$ [32]. That simplified load evaluation method applies to a surface crack density $< 10 - 15\%$ (in the percentage of cracked surface grains); crack length $a > 50$ $\mu m$(i.e. $1 - 2$ times the grain size); while the 3D crack front remains mostly semi-circular [33].

Our model correctly captures both the average crack growth rate and crack growth rate scattering observed in the indicated experimental conditions. Fig. 5 includes up to 30 different cracks analyzed at up to 40 FABIME test arrests. The model results closely follow the validation test results over a broad range of stress intensity factors and crack length ranges, which strongly supports the Stage Ii scenario proposed in Section 2.1 and the related physical (not adjusted) parameters listed in Table 1. The calculation results are generally conservative, especially for $K > 10$ $MPa\sqrt{m}$ as shown in Fig. 5.

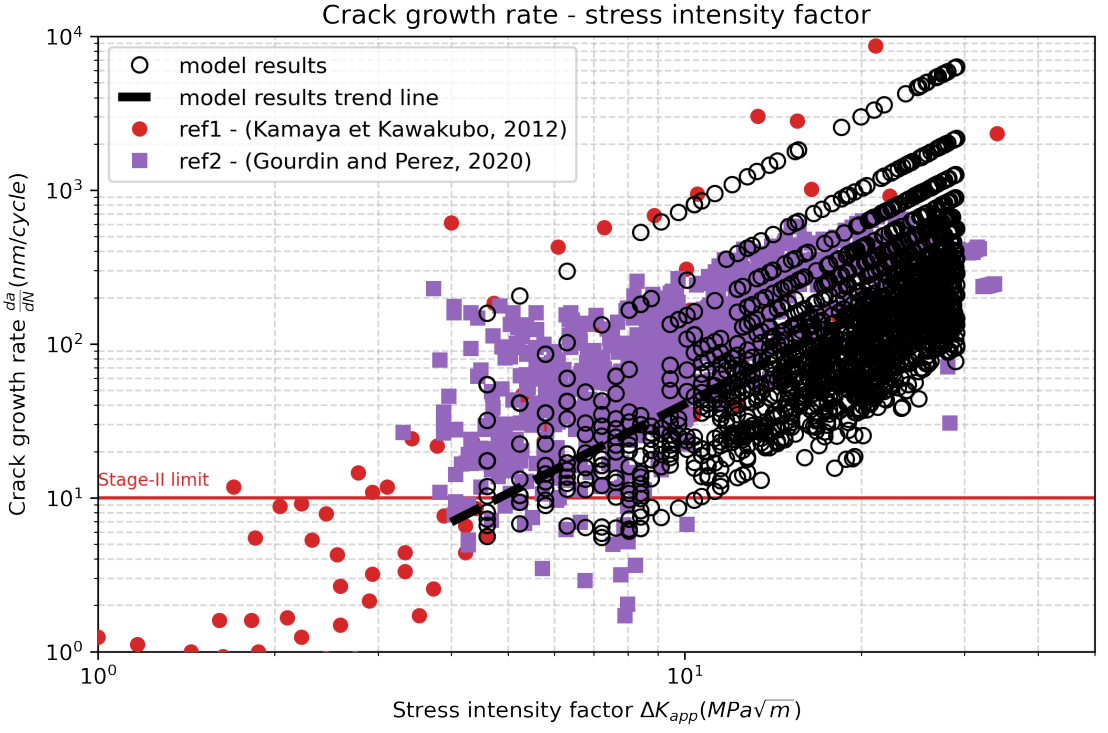


**Figure 5:** Stage II crack growth rate versus stress intensity factor. The open symbols are modeling results; the solid symbols represent two distinct sets of experimental results [30, 34]. The dashed line corresponds to the average, modeling trend curve. The model allows predicting both the average crack growth rate and scattering, in consistency with corresponding experimental evidence. The modeling trend curve (dashed line) cuts the Stage II limit at $4 - 5$ $MPa\sqrt{m}$ in agreement with the stress intensity factor threshold of Stage II crack growth of series 300 steels.

One crack size $a$ versus $N$ evolution example considering every potential crack propagation path (or EBSD data line) is then shown in Fig. 6. These calculation results allow calculating the fatigue lifetime contribution associated with Stage II crack propagation. The fatigue lifetime here is simply set equal to the number of cycles to achieve a crack propagation range[1] $a = 1000$ $\mu m$.

[1]This value is somewhat arbitrary, though taking a larger $a_{crit}$ range yields minimal fatigue lifetime change.

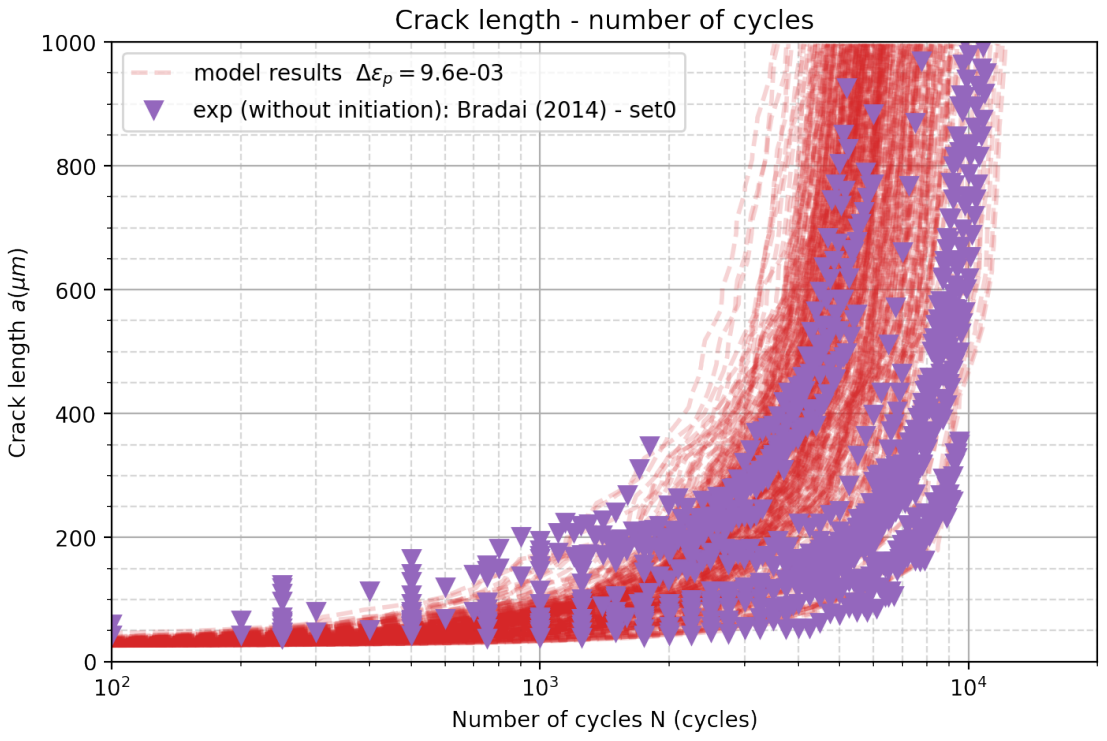


**Figure 6:** The crack depth versus the number of cycles along different crack paths. The thin dashed lines correspond to individual crack-path propagation cases. The calculation results are consistent with the experimental FABIME results [29].

The theoretical fatigue lifetime results are then plotted with respect to various total applied strain range levels and further compared with applicable datasets [34–37], in Fig. 7. Stage II-related fatigue lifetime and its scattering markedly increase with decreasing loading levels, considering the logarithmic scale utilized. This well-known trend actually reflects the non-linear grain size and orientation effects implied by Eq. (3). Theoretical Fig. 7 results are consistent with their experimental counterparts for loading amplitude sitting above a critical value ($N_f < 10^4$ cycles or $\Delta\epsilon_p > 7 \times 10^{-3}$ yielding 50% failure probability). The calculation results markedly deviate from the reference datasets, however, for decreasing loading amplitude. We therefore conclude that the fatigue lifetime (laboratory test specimens case) is crack-propagation-controlled for $\Delta\epsilon_p > 6 \times 10^{-3}$ and crack-initiation-controlled for $\Delta\epsilon_p < 4 \times 10^{-3}$. In the intermediate crack load range, the fatigue lifetime is controlled by both crack initiation and propagation. Fig. 7 results thus highlight a major transition effect, that can significantly influence the applicable fatigue design procedures. Components including initial crack-like defects (like machining marks for example) bear negligible Stage 0 and 1 (crack initiation) contribution, for example. In that case, the corresponding fatigue lifetime is mostly crack-propagation controlled and follows Fig. 7 simulation results (open red symbols), rather than the usual fatigue dataset (solid symbols).

## 4. Conclusions

The fatigue lifetime contribution of Stage II crack growth is here evaluated based on its governing plasticity mechanisms. Our approach allows direct comparison with various sets of applicable experimental data obtained on macroscopic specimens.

Stage II crack growth rate $da/dN$ is evaluated based on the cyclic plasticity mechanisms controlling the crack-tip opening displacements (CTOD) and tip-related, nucleation of nano-cavities (see Section 2). The micro (single grain) to macro (poly-crystal) scale transition is implemented by applying systematic variations of the model entries from applicable EBSD data (maps). The main conclusions drawn from the present theoretical investigations are as follows:

- Our Stage II crack model combines continuous, tip-related plastic glide and the periodic, discontinuous nucleation of nano-cavities along the crack front. That scenario is fully compatible with (discontinuous) striation contrast

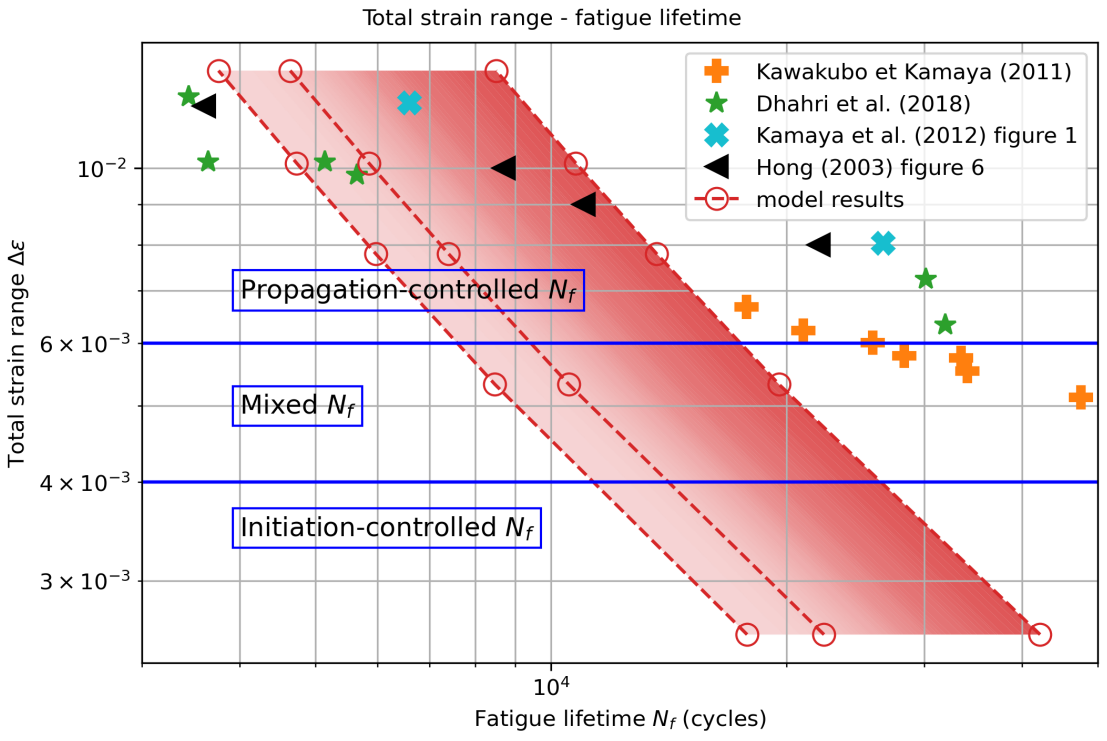


**Figure 7:** Stage II related contribution to fatigue lifetime versus total strain range in a poly-crystalline series 300 steel. The three represented curves are associated with 1%, 10% and 90% failure probability respectively. The solid symbols correspond to experimental measurements from macroscopic fatigue tests in [34–37].

in the fracture surface and strongly supported by corresponding validation results, over a wide range of crack lengths and loading amplitude (c.f. Fig. 7).

- Theoretical Stage II fatigue lifetime amplitude and related fatigue lifetime-scattering increase with decreasing plastic strain range $\Delta\epsilon_p$. These calculation results are again consistent with well-known experimental trends; which we ascribe to the non-linear crack-tip opening displacement dependence on $\Delta\epsilon_p$ and $D_g$ implied by Eq. (1).
- The grain-to-grain size $D_g$ and disorientation variations along the theoretical crack paths appear to be the main contributing cause for the crack growth rate $da/dN$ scattering.
- Our calculation results highlight a major transition effect: the fatigue lifetime is crack-propagation controlled above $\Delta\epsilon_p = 7 \times 10^{-3}$ and crack-initiation controlled below $\Delta\epsilon_p = 7 \times 10^{-3}$.
- Stage II lifetime results (c.f. Fig. 7 open red symbols) are directly applicable to components including initial crack-like defects. This is a major consequence in terms of fatigue design practices, in the context of fusion reactor technology.

Unlike many fatigue life models, our computational approach also allows for generating fatigue design data applicable to various practical situations, including temperature evolutions and different environment mediums (vacuum, corrosive atmospheres, etc). For example, a cohesive energy (parameter $\gamma_{surf}$) increase would produce a slower crack propagation rate and a correspondingly longer fatigue lifetime.

Our model involves very modest calculation resources while providing a comprehensive estimation of the fatigue-life governing causes, especially in cases where laboratory testing is unavailable or prohibitive. This work is adapted to austenitic stainless steels but can also be adapted to various alloys including tungsten and ferritic steels, representing important classes of structural nuclear materials.

## 5. Acknowledgements

This work has been carried out within the framework of the EUROfusion Consortium and has received funding from the Euratom research and training program 2014-2018 and 2019-2020 EDDI under Grant Agreements No. 633053 and No. 755039. The views and opinions expressed herein do not necessarily reflect those of the European Commission. The authors thank C. Gourdin and G. Perez from CEA/LISN for the FABIME fatigue test results reported in this paper.

## 6. Data Availability

The raw data required to reproduce these findings will be made available on request. The processed data required to reproduce these findings will be made available on request.

## References

[1] T. Kruml, J. Pola´k, K. Obrtli´k, S. Degallaix, Dislocation structures in the bands of localised cyclic plastic strain in austenitic 316L and austenitic-ferritic duplex stainless steels, Acta Materialia 45 (12) (1997) 5145–5151. doi:10.1016/S1359-6454(97)00178-X.
URL https://www.sciencedirect.com/science/article/pii/S135964549700178X

[2] J. Man, K. Obrtlík, C. Blochwitz, J. Polák, Atomic force microscopy of surface relief in individual grains of fatigued 316L austenitic stainless steel, Acta Materialia 50 (15) (2002) 3767–3780. doi:10.1016/S1359-6454(02)00167-2.
URL https://www.sciencedirect.com/science/article/pii/S1359645402001672

[3] J. Man, T. Vystavěl, A. Weidner, I. Kuběna, M. Petrenec, T. Kruml, J. Polák, Study of cyclic strain localization and fatigue crack initiation using FIB technique, International Journal of Fatigue 39 (2012) 44–53. doi:10.1016/j.ijfatigue.2011.05.002.
URL https://www.sciencedirect.com/science/article/pii/S0142112311001150

[4] M. Bao-Tong, C. Laird, Overview of fatigue behavior in copper single crystals—I. Surface morphology and stage I crack initiation sites for tests at constant strain amplitude, Acta Metallurgica 37 (2) (1989) 325–336. doi:10.1016/0001-6160(89)90217-4.
URL https://www.sciencedirect.com/science/article/pii/0001616089902174

[5] J. Ahmed, A. J. Wilkinson, S. G. Roberts, Electron channelling contrast imaging characterization of dislocation structures associated with extrusion and intrusion systems and fatigue cracks in copper single crystals, Philosophical Magazine A 81 (6) (2001) 1473–1488, publisher: Taylor & Francis _eprint: https://doi.org/10.1080/01418610108214358. doi:10.1080/01418610108214358.
URL https://doi.org/10.1080/01418610108214358

[6] K. Katagiri, A. Omura, K. Koyanagi, J. Awatani, T. Shiraishi, H. Kaneshiro, Early stage crack tip dislocation morphology in fatigued copper, Metallurgical Transactions A 8 (11) (1977) 1769–1773. doi:10.1007/BF02646881.
URL https://doi.org/10.1007/BF02646881

[7] G. V. Prasad Reddy, R. Sandhya, K. Laha, C. Depres, C. Robertson, A. K. Bhaduri, The effect of the location of stage-I fatigue crack across the persistent slip band on its growth rate – A 3D dislocation dynamics study, Philosophical Magazine 97 (16) (2017) 1265–1280. doi:10.1080/14786435.2017.1294269.
URL https://www.tandfonline.com/doi/full/10.1080/14786435.2017.1294269

[8] C. Déprés, Z. Yang, C. Robertson, Stage-II fatigue crack growth model from 3D dislocation dynamics simulations, Philosophical Magazine 102 (6) (2022) 504–521, publisher: Taylor & Francis _eprint: https://doi.org/10.1080/14786435.2021.2009135. doi:10.1080/14786435.2021.2009135.
URL https://doi.org/10.1080/14786435.2021.2009135

[9] M. Verdier, M. Fivel, I. Groma, Mesoscopic scale simulation of dislocation dynamics in fcc metals: Principles and applications, Modelling and Simulation in Materials Science and Engineering 6 (6) (1998) 755–770, publisher: IOP Publishing. doi:10.1088/0965-0393/6/6/007.
URL https://doi.org/10.1088/0965-0393/6/6/007

[10] C. Déprés, C. F. Robertson *, M. C. Fivel, Low-strain fatigue in AISI 316L steel surface grains: a three-dimensional discrete dislocation dynamics modelling of the early cycles I. Dislocation microstructures and mechanical behaviour, Philosophical Magazine 84 (22) (2004) 2257–2275. doi:10.1080/14786430410001690051.
URL http://www.tandfonline.com/doi/abs/10.1080/14786430410001690051

[11] C. Déprés, C. F. Robertson, M. C. Fivel, Low-strain fatigue in 316L steel surface grains: a three dimension discrete dislocation dynamics modelling of the early cycles. Part 2: Persistent slip markings and micro-crack nucleation, Philosophical Magazine 86 (1) (2006) 79–97, publisher: Taylor & Francis _eprint: https://doi.org/10.1080/14786430500341250. doi:10.1080/14786430500341250.
URL https://doi.org/10.1080/14786430500341250

[12] M. Fivel, C. Déprés, An easy implementation of displacement calculations in 3D discrete dislocation dynamics codes, Philosophical Magazine 94 (2014) 3206–3214. doi:10.1080/14786435.2014.949326.

[13] G. V. Prasad Reddy, C. Robertson, C. Déprés, M. Fivel, Effect of grain disorientation on early fatigue crack propagation in face-centred-cubic polycrystals: A three-dimensional dislocation dynamics investigation, Acta Materialia 61 (14) (2013) 5300–5310. doi:10.1016/j.actamat.2013.05.021.
URL https://www.sciencedirect.com/science/article/pii/S1359645413003893

[14] C. Déprés, MODÉLISATION PHYSIQUE DES STADES PRÉCURSEURS DE L'ENDOMMAGEMENT EN FATIGUE DANS L'ACIER INOXYDABLE AUSTÉNITIQUE 316L, Ph.D. thesis, INSTITUT NATIONAL POLYTECHNIQUE DE GRENOBLE, Grenoble (2004).

[15] C. Robertson, G. V. Prasad Reddy, C. Déprés, M. Fivel, Effect of Grain Disorientation on Early Fatigue Crack Propagation in FCC Polycrystals: Dislocation Dynamics Simulations and Corresponding Experimental Validation, Transactions of the Indian Institute of Metals 69 (2) (2016)

477–481. doi:10.1007/s12666-015-0754-y.
URL https://doi.org/10.1007/s12666-015-0754-y

[16] T. Mura, A theory of fatigue crack initiation, Materials Science and Engineering: A 176 (1) (1994) 61–70, number: 1. doi:10.1016/0921-5093(94)90959-8.
URL https://www.sciencedirect.com/science/article/pii/0921509394909598

[17] C. Déprés, G. Prasad Reddy, C. Robertson, M. Fivel, An extensive 3D dislocation dynamics investigation of stage-I fatigue crack propagation, Philosophical Magazine 94 (36) (2014) 4115–4137, publisher: Taylor & Francis _eprint: https://doi.org/10.1080/14786435.2014.978830. doi:10.1080/14786435.2014.978830.
URL https://doi.org/10.1080/14786435.2014.978830

[18] R. Pippan, A. Hohenwarter, Fatigue crack closure: a review of the physical phenomena, Fatigue & Fracture of Engineering Materials & Structures 40 (4) (2017) 471–495, _eprint: https://onlinelibrary.wiley.com/doi/pdf/10.1111/ffe.12578. doi:10.1111/ffe.12578.
URL https://onlinelibrary.wiley.com/doi/abs/10.1111/ffe.12578

[19] D. O. Harris, H. L. Dunegan, Continuous monitoring of fatigue-crack growth by acoustic-emission techniques: Purpose of this investigation was to further explore the relationship between crack-growth characteristics and acoustic-emission variables such as instrumentation gain and sensor frequency. The threshold conditions for crack detection were also investigated, Experimental Mechanics 14 (2) (1974) 71–81, number: 2. doi:10.1007/BF02323130.
URL http://link.springer.com/10.1007/BF02323130

[20] V. Moorthy, T. Jayakumar, B. Raj, Influence of micro structure on acoustic emission behavior during stage 2 fatigue crack growth in solution annealed, thermally aged and weld specimens of AISI type 316 stainless steel, Materials Science and Engineering: A 212 (2) (1996) 273–280, number: 2. doi:10.1016/0921-5093(96)10206-9.
URL https://linkinghub.elsevier.com/retrieve/pii/0921509396102069

[21] L. De Baglion, J. Mendez, Low cycle fatigue behavior of a type 304L austenitic stainless steel in air or in vacuum, at 20 °C or at 300 °C: Relative effect of strain rate and environment, Procedia Engineering 2 (1) (2010) 2171–2179. doi:10.1016/j.proeng.2010.03.233.
URL https://www.sciencedirect.com/science/article/pii/S1877705810002341

[22] T. Takeda, Y. Shindo, F. Narita, Vacuum crack growth behavior of austenitic stainless steel under fatigue loading, Strength of Materials 43 (5) (2011) 532–536. doi:10.1007/s11223-011-9324-7.
URL https://doi.org/10.1007/s11223-011-9324-7

[23] R. Alain, P. Violan, J. Mendez, Low cycle fatigue behavior in vacuum of a 316L type austenitic stainless steel between 20 and 600°C Part I: Fatigue resistance and cyclic behavior, Materials Science and Engineering: A 229 (1) (1997) 87–94, number: 1. doi:10.1016/S0921-5093(96)10558-X.
URL https://www.sciencedirect.com/science/article/pii/S092150939610558X

[24] P. Lukáš, Fatigue Crack Nucleation and Microstructure (Jan. 1996). doi:10.31399/asm.hb.v19.a0002355.
URL https://dl.asminternational.org/handbooks/edited-volume/34/chapter/451135/Fatigue-Crack-Nucleation-and-Microstr

[25] J. R. Rice, D. C. Drucker, Energy changes in stressed bodies due to void and crack growth, International Journal of Fracture Mechanics 3 (1) (1967) 19–27. doi:10.1007/BF00188642.
URL https://doi.org/10.1007/BF00188642

[26] S. Suresh, Fatigue of Materials, Cambridge University Press, 1998, google-Books-ID: j4w6frFAiQcC.

[27] A. Van der Ven, The thermodynamics of decohesion, Acta Materialia 52 (5) (2004) 1223–1235. doi:10.1016/j.actamat.2003.11.007.
URL https://linkinghub.elsevier.com/retrieve/pii/S1359645403007006

[28] C. P. Blankenship Jr, E. A. Starke Jr, THE FATIGUE CRACK GROWTH BEHAVIOR OF THE Al—Cu—Li ALLOY WELDALITE 049, Fatigue & Fracture of Engineering Materials & Structures 14 (1) (1991) 103–114, _eprint: https://onlinelibrary.wiley.com/doi/pdf/10.1111/j.1460-2695.1991.tb00646.x. doi:10.1111/j.1460-2695.1991.tb00646.x.
URL https://onlinelibrary.wiley.com/doi/abs/10.1111/j.1460-2695.1991.tb00646.x

[29] S. Bradaï, C. Gourdin, C. Gardin, Study of Crack Propagation Under Fatigue Equibiaxial Loading, in: Volume 5: High-Pressure Technology; ASME NDE Division; 22nd Scavuzzo Student Paper Symposium and Competition, American Society of Mechanical Engineers, Anaheim, California, USA, 2014, p. V005T11A013. doi:10.1115/PVP2014-28417.
URL https://asmedigitalcollection.asme.org/PVP/proceedings/PVP2014/46025/Anaheim,%20California,%20USA/283861

[30] C. Gourdin, G. Perez, Réalisation d'Essais de Fatigue Equibiaxiaux dans le cadre de l'action DDC-IC 2020 (2020) 29.

[31] C. Gourdin, G. Perez, Réalisation d'Essais de Fatigue Equibiaxiaux dans le cadre de l'action DDC-IC 2019, Tech. rep., CEA, France (2019).

[32] S. Shanmugham, P. K. Liaw, Detection and Monitoring of Fatigue Cracks, ASM Handbook 19 (1996) 134. doi:10.31399/asm.hb.v19.a0002363.
URL https://dl.asminternational.org/handbooks/edited-volume/34/chapter/451940/Detection-and-Monitoring-of-Fatigue-C

[33] C. Robertson, S. Chaise, Essai de fatigue thermique avec contrainte statique de traction sur un acier austénitique, CEA Technical Report DMN/SRMA/LC2M/NT/2006-2816/A (2006), CEA, France (2006).

[34] M. Kamaya, M. Kawakubo, Strain-based modeling of fatigue crack growth – An experimental approach for stainless steel, International Journal of Fatigue 44 (2012) 131–140. doi:10.1016/j.ijfatigue.2012.05.006.
URL https://linkinghub.elsevier.com/retrieve/pii/S0142112312001776

[35] M. Kawakubo, M. Kamaya, Fatigue Life Prediction of Stainless Steel under Variable Loading (Damage Factors Determining Fatigue Life and Damage Evaluation for Two-Step Test), Journal of the Society of Materials Science, Japan 60 (10) (2011) 871–878, number: 10. doi:10.2472/jsms.60.871.
URL http://www.jstage.jst.go.jp/article/jsms/60/10/60_10_871/_article/-char/ja/

[36] H. Dhahri, C. Gourdin, G. Perez, S. Courtin, J.-C. Le Roux, H. Maitournam, PWR EFFECT ON CRACK INITIATION UNDER EQUI-BIAXIAL LOADING: DEVELOPMENT OF THE EXPERIMENT, Procedia Engineering 213 (2018) 571–580. doi:10.1016/j.proeng.2018.02.052.
URL https://linkinghub.elsevier.com/retrieve/pii/S1877705818302832

[37] S.-G. Hong, S. Yoon, S.-B. Lee, The effect of temperature on low-cycle fatigue behavior of prior cold worked 316L stainless steel, International Journal of Fatigue 25 (9) (2003) 1293–1300, number: 9. doi:10.1016/S0142-1123(03)00154-3.
URL https://www.sciencedirect.com/science/article/pii/S0142112303001543